

https://dspace.org/

Atomisation of Ti6Ta15Zr02Ru5Cu wt for additive manufacturing for biomedical applications

Ngwakoana Phala; Claudia Polese; T Choma; H Moller; L Zrodowski ...

https://hdl.handle.net/10539/39708
DOAJ

Downloaded from a DSpace repository. https://dspace.org/

Atomisation of Ti-6Ta-1.5Zr-0.2Ru-5Cu (wt%) for additive manufacturing for biomedical applications

Ngwakoana Phala[1*], *Claudia* Polese[2], *Tomasz* Choma[3], *Hein* Möller[4], *Łukasz* Żrodowski[3] and *Lesley* Cornish[1]
[1]School of Chemical and Metallurgical Engineering and DSI-NRF CoE in Strong Materials, University of the Witwatersrand, South Africa
[2]School of Mechanical, Aeronautical and Industrial Engineering, University of the Witwatersrand, South Africa
[3]AMAZEMET, Warsaw, Poland
[4]Advanced Materials Division, Mintek, South Africa

Abstract. The use of titanium alloys is growing fast as people have longer life expectancies and small, customised, biomedical implants, especially in dental applications, encourage the use of additive manufacturing (AM) to shape them. The Ti-6Ta-1.5Zr-0.2Ru-5Cu (wt%) alloy has been identified as a potential alloy for biomedical applications. Since laser powder bed fusion (L-PBF) requires starting powders to be spherical and within a 10-100 µm size range, the Ti-6Ta-1.5Zr-0.2Ru-5Cu (wt%) powder was ultrasonically atomised and then analysed by a Malvern Mastersizer, XRD and SEM-EDX to ascertain that it met the requirements of L-PBF.

1 Introduction

Titanium alloys are used in biomedical applications, including dental uses, due to their high strength, low Young's modulus, excellent corrosion resistance and biocompatibility, and their ability to bond with bone (i.e. osseointegration) [1]. The Ti-6Al-4V alloy and commercially pure titanium (CP-Ti) have been used in aerospace for engine components [2]. Both these materials started to replace stainless steels and cobalt-based alloys in many biomedical applications since the 1970s [3] and are considered compatible due to their excellent combination of tensile and fatigue performance as well as biocompatibility [4]. However, there are some concerns about Ti-6Al-4V since the alloying elements, aluminium and vanadium, are considered toxic [5], whereas CP-Ti does not have sufficient strength for load bearing implant applications [6].

Using Ti-6Al-4V as the (α+β) reference, recent studies were done to replace Al and V with non-toxic elements for α+β stabilising, with zirconium and tantalum being proposed as the potential non-toxic alloying elements [7]. Copper was chosen because Cu additions to Ti alloys promote antibacterial properties [8, 9]. According to Liu et al. [9], the Cu content must

* Correspondant author: 820850@students.wits.ac.za

© The Authors, published by EDP Sciences. This is an open access article distributed under the terms of the Creative Commons Attribution License 4.0 (https://creativecommons.org/licenses/by/4.0/).

be at least 5 wt% to obtain stable antibacterial activity and balanced mechanical properties. The Ti-6Ta-1.5Zr-0.2Ru-5Cu (wt%) alloy was developed as a new potential (α+β) Ti alloy for dental applications [10]. Tantalum was chosen to replace V as a β stabiliser and Zr as a solution-hardening element, with Zr also contributing to the formation of a protective passive film to give good corrosion resistance [7]. Ruthenium was added to enhance corrosion resistance without changing the microstructure and is also non-toxic to living tissues [11].

Additive manufacturing (AM) was developed four decades ago and more recently has become useful and cost effective for fabricating small, geometrically complex objects [12]. The AM process involves fabrication of an object by depositing materials layer-by-layer following a three-dimensional model generated using computer-aided drawing. Hence, AM offers the added advantage of fabricating fully compatible and accurate biomedical components [13]. Conventional methods (such as casting and powder metallurgy) require multiple steps which limit the time for modification of the final product, and it is difficult to produce complex shapes.

AM includes different technologies; for this work, the laser powder-based fusion (L-PBF) method was selected because it can be used to manufacture almost all metal alloys and has a low direct cost [14]. L-PBF requires the starting powder to be spherical and within a typical size range of 15-45 µm for easy flowability and spreadability [15], although AMAZEMET stated that the powder could be in the size range of 10-100 µm [16]. The rePowder ultrasound atomisation system (AMAZEMET) was used to atomise the powder in small batches [16], using common laboratory conditions and can generate high purity spherical powders.

Ultrasound atomisation is a liquid to solid process, where the material can either be melted in a crucible if the material is non-reactive and has a low melting point (e.g., Sn, Zn, Mg, Pb and Al alloys), and can be poured into the vibrating element or melted directly into the sonotrode if the material is highly reactive or has a high melting point (e.g., alloys based on Fe, Ti and Pt) [16]. The main principle of ultrasound atomisation depends on the amplitude and the surface wettability of the material [16]. Increasing the amplitude makes the liquid droplets smaller, and their size also depends on the frequency used and the properties of the liquid itself. These droplets are ejected from the melt within the thin film of liquid on the sonotrode surface [16]. The Particle Size Distribution (PSD) of ultrasound atomisation is narrow which means that up to 80% of the manufactured powder can be used [16]. The main factor that influences the PSD of the resulting powder is the frequency used. For L-PBF, a 40 kHz frequency is suitable for powder with a D_{50} (average particle size) of 45-60 µm. The atomisation is carried under inert gas using an electric arc or focused plasma [17].

2 Experimental procedure

Pure elemental powders of: Ti <45 µm, Ta < -60+100 mesh, Zr = APS 2-3 µm, Ru <45 µm and Cu <45 µm particle sizes were mixed in the ratio for Ti-6Ta-1.5Zr-0.2Ru-5Cu (wt%) for a total mass of 100 g. The powders were blended in a WAB T2C Turbula mixer to obtain a good mixture, followed by compaction with an Instron 1175 testing machine with the maximum load of 70 kN and cross-head speed of 20 mm/min. Ultrasonic atomisation was done using a rePower system [16], with a molybdenum alloy sonotrode at 40 kHz, with fixed 155A current and 100-130% amplitude of the sonotrode at 180-280W, and 7 L/min argon gas flow, with the blower set at 13-17% maximum power. The whole process was carried out in an argon atmosphere. Powder produced was collected in an air lock container which was sealed in argon for safe handling. Fig 1. shows the rePower system used [16]. A Malvern

Mastersizer was used for particle analysis and the average of the three runs was recorded before and after the atomisation. The powder was characterised by scanning electron microscopy-energy dispersive X-ray spectroscopy (SEM-EDX) to determine the morphology and elemental compositions before and after atomisation. X-ray diffraction (XRD) with Co radiation was used to determine the phases in the powder before and after atomisation. The atomised powder was mounted in epoxy hot mounting resin and ground on 1200 grit grinding paper and polished to ~1µm and the cross sections of the particles were characterised by SEM-EDX.



Fig 1. Fully equipped rePower system [16].

3 Results and discussion

SEM back scattered electron images of elemental powders show irregular shapes, Fig. 2. In Fig. 2(b), the order of contrasts from lightest to darkest (based on atomic number) was Ta, Ru, Zr, Cu and Ti.

Fig. ***3*** shows X-ray mapping results of the blended powder, which indicates the sizes and morphologies of the different elemental powders. The titanium powder particles are larger compared to Ta and Cu, which tended to be concentrated together. The Ru and Zr powder particles were barely discernible due to their low proportions.

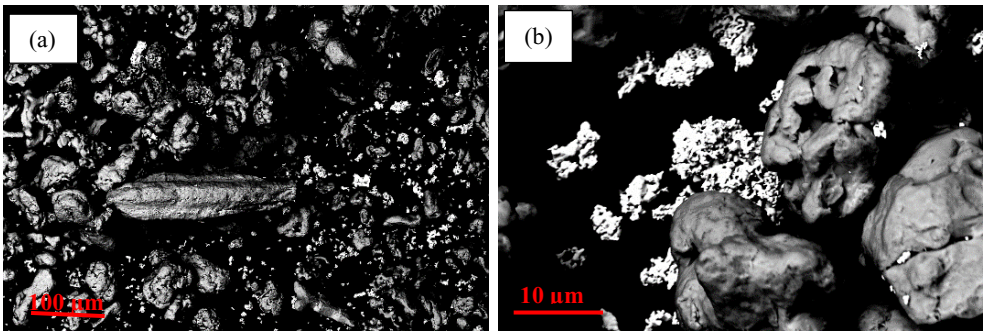


Fig. 2. SEM-BSE images of blended elemental powders of Ti, Ta, Zr, Ru and Cu before atomisation: (a) lower and (b) higher magnification.

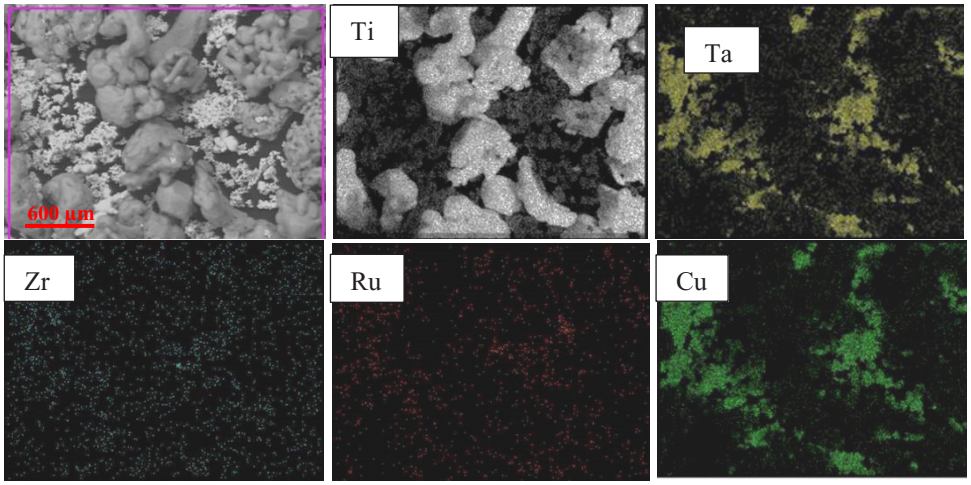


Fig. 3. Elemental EDX maps of the elemental blended powder of Ti, Ta, Zr, Ru and Cu before atomisation.

SEM-SE images of powders after atomisation are given in Fig. 4, showing that the powder was spherical and within the size range required for L-PBF [17], although there was a large irregular particle (indicated by the arrow) in Fig. 4 (b).

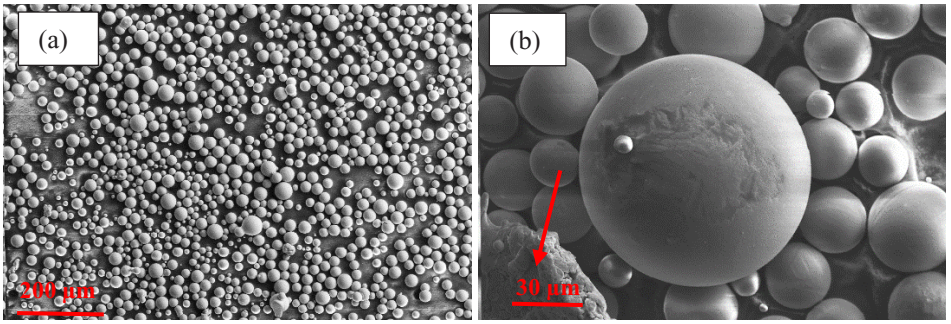


Fig. 4. SEM-SE images of Ti-6Ta-1.5Zr-0.2Ru-5Cu (wt%) powder after atomisation: (a) lower and (b) higher magnification, showing large spherical particles and an irregular particle.

The EDX mapping results of powder particles after atomisation are given in Fig. 5. Alloying occurred during atomisation and the distribution of elements was homogeneous.

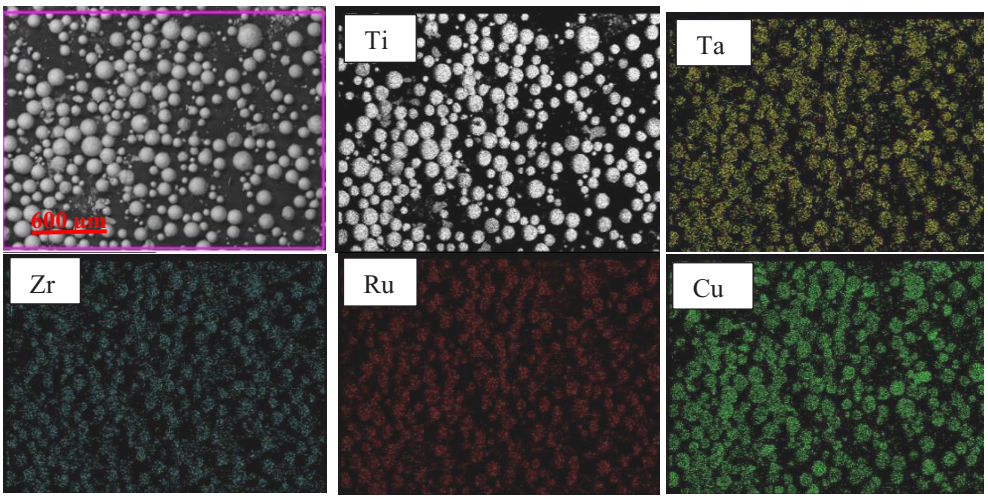


Fig. 5. EDX mapping of the atomised Ti-6Ta-1.5Zr-0.2Ru-5Cu (wt%) atomised powder.

Fig. 6 shows SEM images of the cross-sections of the atomised powder at lower and higher magnification showing minor internal porosity, an irregular particle with regions of different compositions (Fig. 6(a)) and dendrites (Fig. 6(b)). Fig. 7 shows the mapping of the cross-sections of the powder. Table 1 shows that the contents were close to the targeted composition, except for Zr which was lower than expected, probably because prior to atomisation, the Zr had been weighed together with the liquid in which it was stored to prevent oxidation. The EDX results of the cross-sections of the irregular powders showed that some particles did not have Zr and Ru. Ruthenium could have been lost because it was the heaviest element and was also in a small proportion.

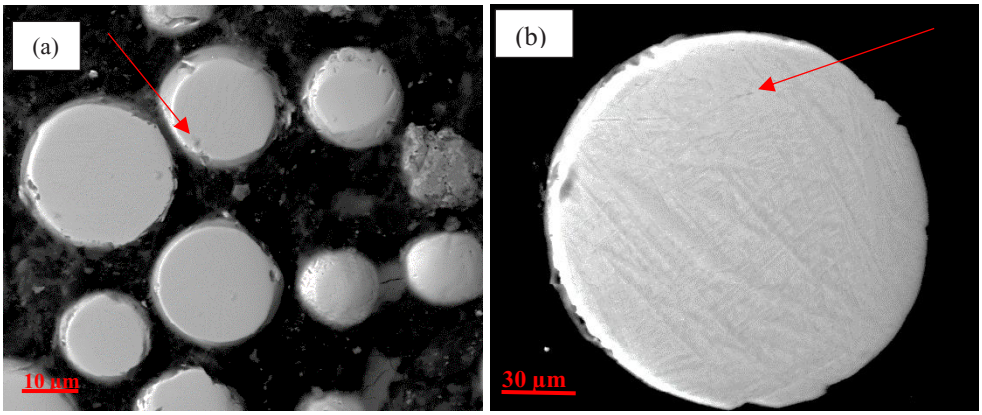


Fig. 6 . SEM-BSE images of cross-sections of Ti-6Ta-1.5Zr-0.2Ru-5Cu (wt%) powder, arrow showing internal porosity.

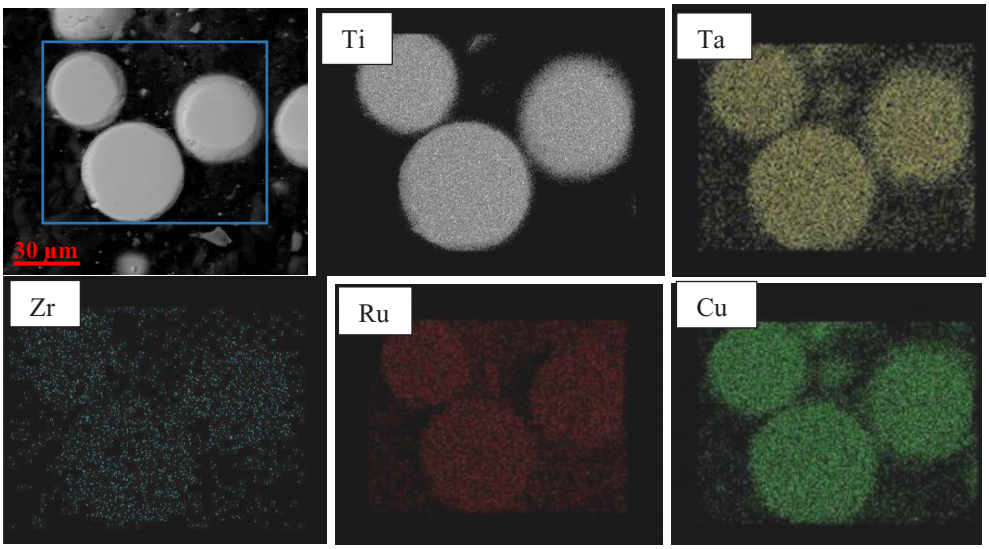


Fig. 7. EDX mapping of cross-sections of a few Ti-6Ta-1.5Zr-0.2Ru-5Cu (wt%) atomised powder particles.

The area shown by the squares in Fig. 8 are examples of the scans on ten different particle cross-sections and the average results are recorded in Table 1. The larger particles had compositions closer to the target than the smaller and irregular particles.

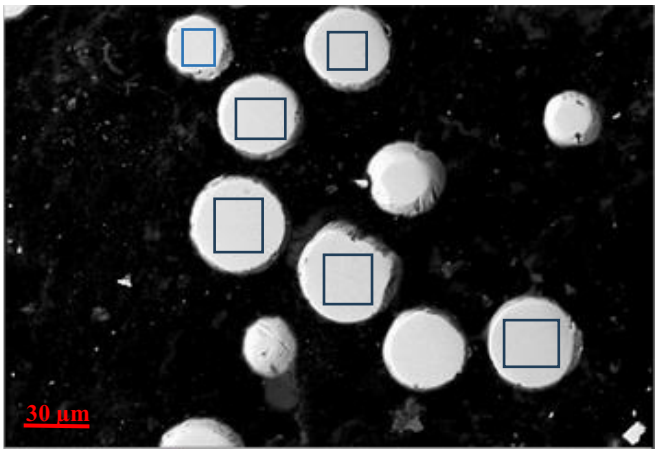


Fig. 8. SEM-BSE image indicating the areas of the EDX analyses within cross-sectioned atomised powder particles.

Table 1. Targeted composition and EDX results for area scans of cross-sections of atomised Ti-6Ta-1.5Zr-0.2Ru-5Cu (wt%) powder particles.

	Ti	**Ta**	**Zr**	**Ru**	**Cu**
Targeted	87.3	6	1.5	0.2	5
Larger spherical particles	88.0 ± 0.4	6.9 ± 0.4	0.1 ± 0.6	0.2 ± 0.1	4.8 ± 0.2
Smaller irregular particles	87.2 ± 0.5	5.2 ± 0.6	0.0 ± 0.0	0.0 ± 0.0	7.6 ± 0.8

Particle size distributions of the blended elemental powder before atomisation are shown in Fig. 9, and Fig. 10 for the alloy powder after atomisation. Fig. 9 has a small peak at ~9 µm with the largest peak at ~50 µm, and another small peak around ~250 µm. Fig. 10 shows that there were no particles below 10 µm and a second peak at ~800 µm after atomisation. EDX of these particles showed that all the targeted elements were present in the large, spherical particles. Fig. 11 shows a large particle formed by agglomeration of smaller particles, which had not been atomised correctly, and this was also observed by Möller et al. [18] who attributed the phenomenon to splintering of the feedstock material before melting. It is likely that the splintered particles, having high surface areas, would combine to form the larger particles and reduce the surface area and energy, even if not atomised properly. Möller et al. [18] also observed composite particles that formed by spattering of liquid that was ejected from the arc and landed on another particle, and in this work is shown as agglomerated small particles of different compositions in Fig. 6(a). This could also explain why some of the irregularly shaped particles had only Ti, Ta, and Cu (Table 1). Fig. 11 shows this, and that some of the spherical particles were included in the agglomeration.

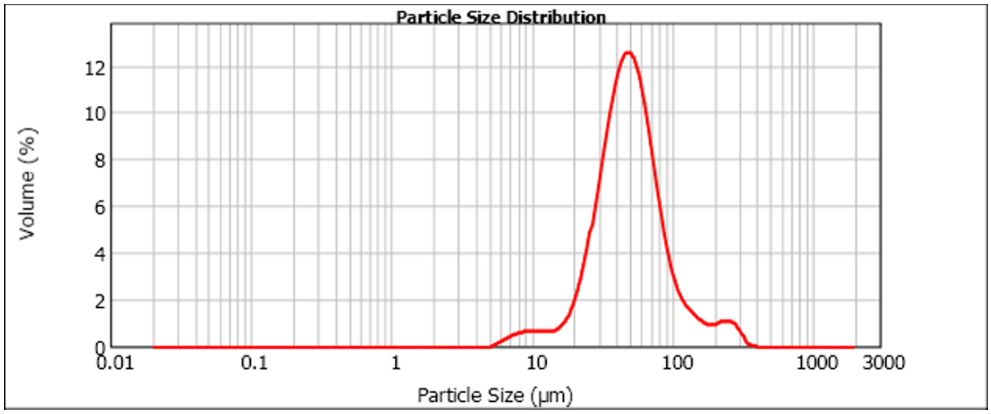


Fig. 9. Particle size distribution of blended elemental powders of Ti, Ta, Zr, Ru and Cu before atomisation.

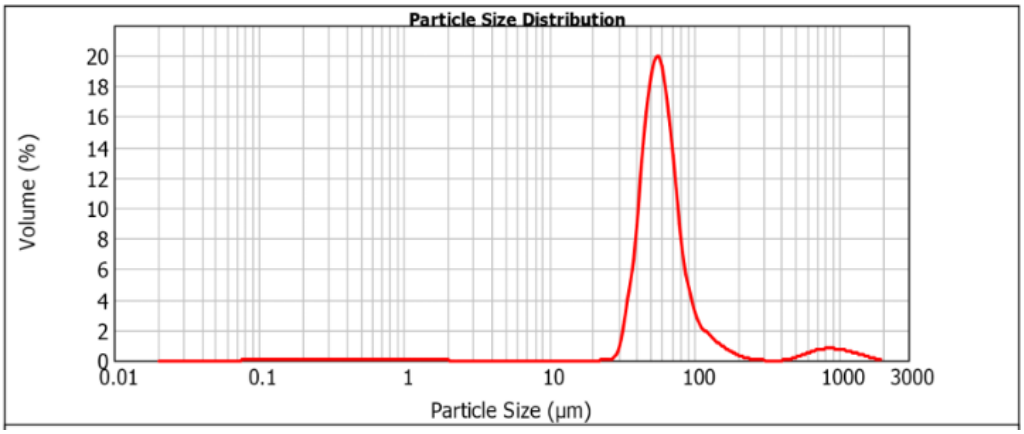


Fig. 10. Particle size distribution of Ti-6Ta-1.5Zr-0.2Ru-5Cu (wt%) powder after atomisation.

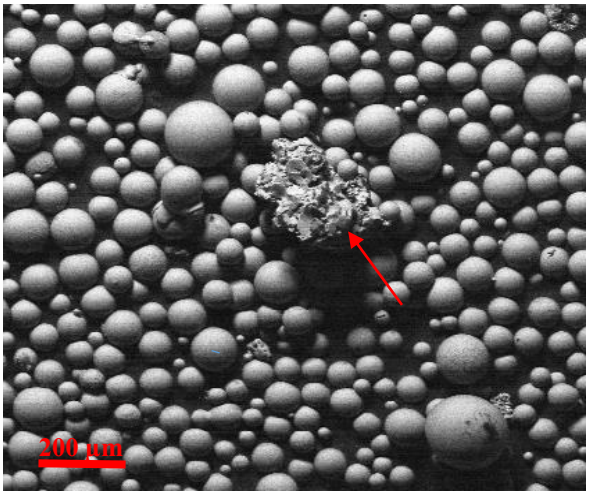


Fig. 11. SEM-SE image showing an agglomeration of splintered particles.

Table 2 shows the summary of the particle size distributions (PSD) before and after atomisation. For both, the D_{50} was within 45-60 µm, where D_{50} is defined as the average particle size of the powder. The PSD of the powder after atomisation could have been narrower if a #200 µm sieve had been used.

Table 2. Average particle size distributions of blended powder and after atomisation.

	D_{10}	**D_{50}**	**D_{90}**
Blended elemental powder	25.1	48.6	100.6
After atomisation	40.7	58.3	106.9

X-ray diffraction (XRD) also showed that alloying occurred during the atomisation. Fig. 12 shows XRD results of the blended elemental powders of Ti, Ta, Zr, Ru and Cu before

atomisation, with major peaks of Ti and a Ta peak. Conversely, Fig. 13, after atomisation, has some different peaks, with Ti_2Cu that gives the antibacterial properties of the alloys [8], which is beneficial for biomedical applications. The Zr and Ru would not be expected to have been detected, since their amounts were below the 4 vol.% detection limit for XRD, although Cu should have been detected, albeit with low peaks. Since the backgrounds were high (small particles), possibly the Cu peaks were lost in the background.

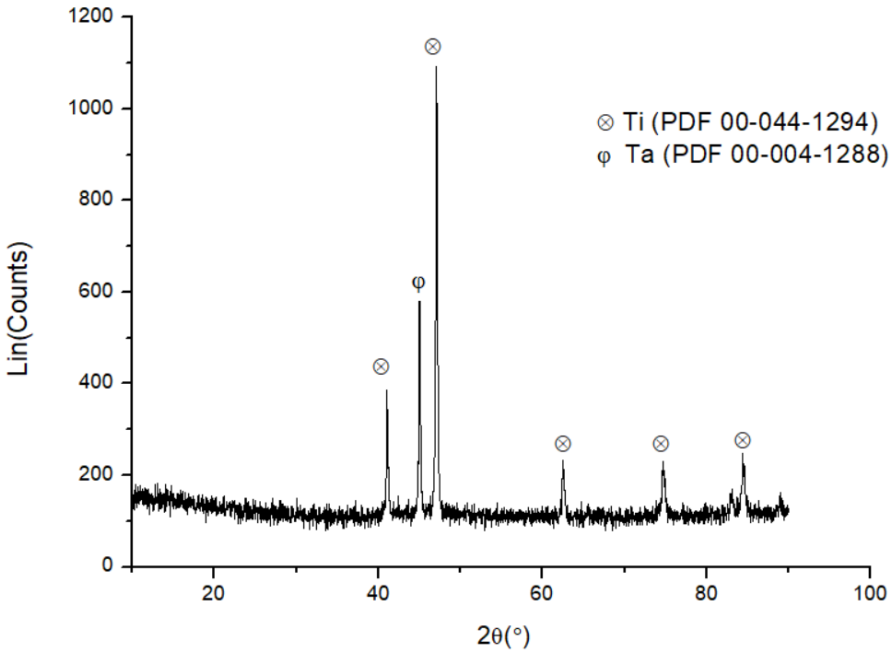


Fig. 12. XRD pattern for blended elemental powder before atomisation.

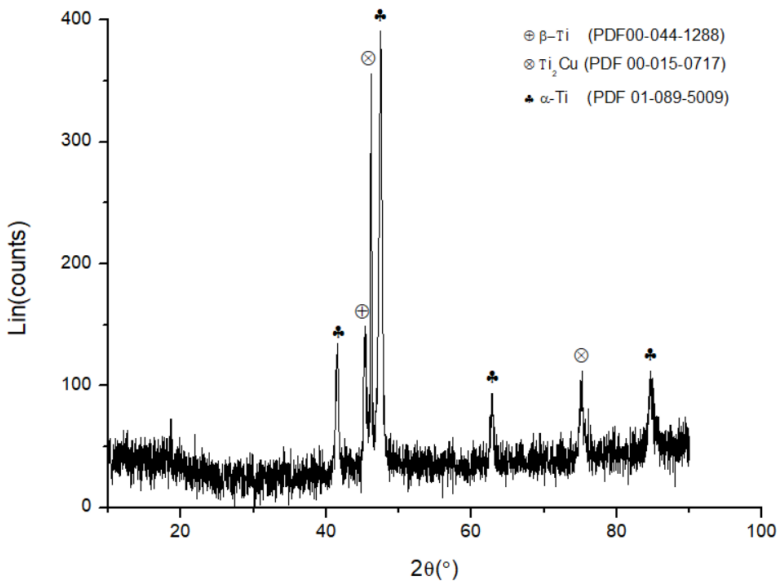


Fig. 13. XRD pattern for Ti-6Ta-1.5Zr-0.2Ru-5Cu (wt%) powder after atomisation.

4 Conclusions

- The powder met the L-PBF specifications of being spherical and with a D_{50} of 58 µm.
- The ultrasonically atomised powder had a narrow particle size distribution. Sieving out the oversized, agglomerated splintered particles would make it an ideal feedstock for Additive Manufacturing technologies.
- The (αTi), (βTi) and Ti_2Cu phases were found by XRD after atomisation.

The authors would like to acknowledge Libo Spotose for developing this alloy, NRF, CoE-SM and the Collaborative Programme on Additive Manufacturing (CPAM) (Contract CSIR-NLC-CPAM-21-MOA-WITS-01) for financial support, Mintek for blending and compaction of the elemental powders, Warsaw University of Technology and AMAZEMET for atomisation of the powder, Letta Ntuli for XRD measurements, and Zaynab Cader for SEM operation.

References

1. C. Leyens and M. Peters. Titanium and Titanium Alloys, Weinheim: Wiley-vch. (2003).
2. I. Inagaki, T. Takechi, Y. Shirai, N. Ariyasu. Application and features of titanium for the aerospace industry. Nippon Steel & Sumitomo Metal Technical Report, Number 106,. pp. 22-27, (2014).
3. D. Mantovani. Shape memory alloys: Properties and biomedical applications. JOM, **52**, pp. 36-44, (2000).

4. J.L. Xu, S.C. Tao, L.Z. Bao, J.M Luo, Y.F. Zheng. Effects of Mo contents on the microstructure, properties and cytocompatibility of the microwave sintered porous Ti-Mo alloys. Mat. Sci. Eng.: C, **97**. pp. 156-165, (2019).
5. V.S.A. Challa, S. Mali, R.D.K. Misra. Reduced toxicity and superior cellular response of preosteoblasts to Ti-6Al-7Nb alloy and comparison with Ti-6Al-4V. J. Biomed. Mat. Res. Part A, **101**, 7, pp. 2083-2089, (2013).
6. N. Soro, H. Attar, E. Brodie, M. Veidt, A. Molotnikov, M.S. Dargusch. Evaluation of the mechanical compatibility of additively manufactured porous Ti–25Ta alloy for load-bearing implant applications. J. Mech. Behav. Biomedi. Mat., **97**, pp. 149-158, (2019).
7. P. Stenlund, O. Omar, U. Brohede, S. Norgren, B. Norlindh, A. Johansson, J. Lausmaa, P. Thomsen, A. Palmquist, Bone response to a novel Ti-Ta-Nb-Zr alloy. Acta Biomat., **20**, pp. 165-175, (2015).
8. E. Zhang, F. Li, H. Wang, J. Liu, C. Wang, M. Li, K. Yang. A new antibacterial titanium–copper sintered alloy: preparation and antibacterial property. Mat. Sci. Eng. C, **33,** 7, pp. 4280-4287, (2013).
9. J. Liu, F. Li, C. Liu, H. Wang, B. Ren, K. Yang, E. Zhang. Effect of Cu content on the antibacterial activity of titanium–copper sintered alloys. Mat. Sci.Eng. C, **35**, pp. 392-400, (2014).
10. L. Spotose. Identifying Ti-Cu-based alloys for biomedical applications, MSc dissertation, University of the Witwatersrand, (2023).
11. C.S. Allardyce, P.J. Dyson. Ruthenium in medicine: current clinical uses and future prospects. Plat. Met. Rev., **45**, 1, pp. 62-69, (2001).
12. P. Ahangar, M.E. Cooke, M.H. Weber, D.H. Rosenzweig. Current biomedical applications of 3D printing and additive manufacturing. Appl. Sci., **9**, 8, pp. 1-23, (2019).
13. A.A Zadpoor. Design for additive bio-manufacturing: From patient-specific medical devices to rationally designed meta-biomaterials. Int. J. Molec. Sci., **18**, 8, pp. 1607-1625, (2017).
14. J. Ni, H. Ling, S. Zhang, Z. Wang, Z. Peng, C. Benyshek, R. Zan, A.K Miri, Z. Li, X. Zhang, J. Lee. Three-dimensional printing of metals for biomedical applications. Mat. Today Bio, **3**, pp. 1-18, (2019).
15. I. Yadroitsev, I. Yadroitsava, A. Du Plessis, E. MacDonald. Fundamentals of Laser Powder Bed Fusion of Metals, pp. 245-276. Amsterdam, The Netherlands: Elsevier, (2021).
16. A novel approach for the production of metal powders with tailored chemical composition: AMEZEMET's rePowder, Powder Metallurgy Review, Winter 2022.
17. L. Żrodowski, R. Wróblewski, T. Choma, B. Morończyk, M. Ostrysz, M. Leonowicz, W. Łacisz, P. Błyskun, J.S. Wróbel, G. Cieślak, B. Wysocki. Novel cold crucible ultrasonic atomization powder production method for 3D printing. Mater., **14**, 10, pp. 2541-2552, (2021).
18. H. Möller, V. Motsweni, L. Zrodowski, T. Choma, Powder characterisation of Pt84-Al11-Cr3-Ru2 superalloy manufactured by ultrasonic atomisation, in Proceedings of the 8th International PGM Conference, 2 – 3 November 2022, Sun City, South Africa (2022).